Experimental Investigation on the Seismic Behaviour of Beam-Column Joints Reinforced with Superelastic Shape Memory Alloys

M. A. Youssef[1], M.S. Alam, and M. Nehdi

Department of Civil and Environmental Engineering, The University of Western Ontario,
London, Ontario, Canada, N6A 5B9

Abstract

Superelastic Shape Memory Alloys (SE SMAs) are unique alloys that have the ability to undergo large deformations and return to their undeformed shape by removal of stresses. This study aims at assessing the seismic behaviour of beam-column joints reinforced with SE SMAs. Two large-scale beam-column joints were tested under reversed cyclic loading. While the first joint was reinforced with regular steel rebars, SE SMA rebars were used in the second one. Both joints were selected from a Reinforced Concrete (RC) building located in the high seismic region of western Canada and designed and detailed according to current Canadian standards. The behaviour of the two specimens under reversed cyclic loading including their drifts, rotations, and ability to dissipate energy were compared. The results showed that the SMA-reinforced beam-column joint specimen was able to recover most of its post-yield deformation. Thus, it would require a minimum amount of repair even after a strong earthquake.

Keywords: beam-column joint, seismic, shape memory alloy, superelasticity, plastic hinge.

---

[1] Corresponding Author. Email: youssef@uwo.ca, Fax: 519-661-3779, Phone: 519-661-2111 Ext.: 88661

1. Introduction

Beam-column joints (BCJs) in RC moment resisting frames are usually considered the weakest link in such a structural system (Park and Paulay 1975). Since the 1970's, design codes started enforcing stricter seismic provisions for the detailing of reinforcing bars in BCJs. However, BCJs remain extremely vulnerable during earthquakes (Saatcioglu et al. 2001). It has been emphasized that earthquake resistant structures need to be sufficiently ductile as it is difficult and costly to build structures that can perform elastically under strong ground motion. In conventional seismic design of RC structures, reinforcing bars are expected to yield in order to dissipate energy resulting in permanent deformations due to the post-yield plastic properties of steel reinforcing bars. If superelastic (SE) SMAs could be used as reinforcing bars, such elite materials can undergo large inelastic deformations and recover their original shape by stress removal mitigating the problem of permanent deformations. This unique property is known as superelasticity,. Hence, when used as reinforcement in critical structural elements along with conventional steel, SMA can undergo large inelastic strains caused by seismic loads, but potentially recover deformations at the end of the earthquake (Saiidi and Wang 2006). Their high strength, large energy hysteretic behaviour, full recovery of strains up to about 8%, and high resistance to corrosion and fatigue make them strong contenders for use in earthquake resistant structures (Wilson and Wesolowsky 2005). In particular, Ni-Ti alloy has been found to be the most promising SMA for seismic applications.

SMAs have gained increased usage in structural applications (Alam et al. 2007a). For instance, Dolce et al. (2004) used SMA bracings for the seismic retrofitting of existing

frames. Maji and Negret (1998) used SMA wires/tendons in prestressed concrete. Indirli et al. (2001) utilized SMA rods for strengthening structures through the application of corrective post-tensioning forces. Inaudi and Kelly (1994), Clark et al. (1995) and others contributed significant analytical and experimental studies on structural displacement control using SMAs. Recent research in the application of SMAs in vibration control includes amongst others the work of DesRoches and Delemont (2002) and Wilde et al. (2000).

Manufacturing of SMA involves overcoming many difficulties, which increases its cost. Adding the fact that the behaviour of large diameter SMA specimens is not well documented in the literature, it was not until 2004 that it found its way as reinforcement in RC structures. Wang (2004) used SMA rods in the plastic hinge area of RC columns and evaluated the seismic performance of these columns. Two ¼-scale spiral RC columns with SMA longitudinal reinforcement in the plastic hinge area were designed for laboratory shake table testing. Each specimen was subjected to a series of scaled motion amplitudes. It was observed that the SMA RC columns were superior to the conventional steel RC columns in limiting relative column top displacement and residual displacements. Also they withstood larger earthquake amplitudes than that of the conventional ones. The shake table data showed that SMA RC columns were able to recover nearly all of the post-yield deformation, thus requiring minimal repair. Alam et al. (2007b) demonstrated the potential of developing smart RC bridges utilizing SMAs as reinforcement and/or prestressing tendons.

In this paper, it is proposed to use SE SMAs as reinforcement in conjunction with steel in RC beam-column joints. Two BCJ specimens have been designed and constructed according to current seismic design standards, and tested under reversed cyclic loading. The prime objective of this study is to investigate the behaviour of concrete BCJ reinforced with SMA in its plastic hinge zone under reversed cyclic loading and compare its performance to that of conventional steel-RC BCJ.

2. Research Significance

RC structures are designed for safety conditions, where earthquake energy is dissipated through yielding of the reinforcement and its inelastic deformation. Structures are allowed to undergo severe damage, which means saving lives at the expense of incurring huge economic losses. Recently this vision has been broadened where the designers no longer want to surrender their creations/constructions. The seismic design of structures has evolved towards performance-based design in which there is need for new structural members and systems that possess enhanced deformation capacity and ductility, higher damage tolerance, decreased residual crack sizes, and recovered or reduced permanent deformations.

The seismic design of ductile moment-resisting frames aims at forcing the structure to respond in a strong column-weak beam action in which plastic hinges are expected to form in the beams at the faces of the columns. The hinging regions are detailed such that yielding of the longitudinal steel bars allows dissipating the earthquake energy.. If SE SMA is used as reinforcement instead of steel in the desired hinge locations of beams, it

will not only be able to dissipate adequate seismic energy, but will also restore its original shape after a seismic event. Because of its higher cost compared to that of other construction materials, SMA longitudinal rebars could be used along with steel rebars at the hinge regions of beams. Such BCJs could allow structural engineers to design connections exhibiting little damage and mitigating post earthquake joint repairs.

3. Experimental Program

Two large-scale BCJ specimens are considered in this study. One is reinforced with regular steel rebars (specimen JBC-1), while the other is reinforced with SMA at the plastic hinge region of the beam along with regular steel in the remaining portion of the joint (specimen JBC-2). Both joints were constructed and tested at the Structures Laboratory of the University of Western Ontario.

3.1 Test specimens

An eight-storey RC building with moment resisting frames was designed and detailed in accordance with Canadian Standards (CSA A23.3-04). The building was assumed to be located in the western part of Canada on firm ground with un-drained shear strength of more than 100 kPa. The elevation and plan of the building are shown in Fig. 1. The design Peak Ground Acceleration (PGA) is 0.54g and the moment frames were designed with a moderate level of ductility. An exterior BCJ was isolated at the points of contra-flexure, from mid-height of fifth floor to mid-height of sixth floor (Joint A in Fig. 1). The size of the BCJ test specimens was reduced by a factor of ¾ to account for the laboratory space and limitations of testing equipments. The forces acting on the joints were also

scaled down by a factor of $(\frac{3}{4})^2$. This factor was chosen to maintain stresses in the scaled models similar to that of the full-scale joint.

The beam and column were designed for maximum moments and shear forces developed considering all possible load combinations. The design column axial force, P, was 620 kN leading to a scaled down P of 350 kN. The detailed design of joints JBC-1 and JBC-2 is given in Fig. 2.

The geometry and longitudinal and transverse reinforcement arrangements of the columns are similar for both BCJ specimens. The reduced cross-section of the columns are 250 mm by 400 mm with 4-M20 (19.5 mm diameter) longitudinal rebars corresponding to a 1.20% reinforcement ratio. The columns are transversely reinforced with M10 (11.3 mm diameter) closed rectangular ties spaced at 80 mm in the joint region and for a distance of ±640 mm from the face of the joint. The spacing of the ties for the remaining length of the columns is 115 mm.

Beams of JBC-1 and JBC-2 are similar in terms of geometry and amount and arrangement of transverse reinforcement. They have different longitudinal reinforcement at the plastic hinge region where JBC-2 utilized SE SMA and JBC-1 had regular steel. The top and bottom longitudinal reinforcement for JBC-1 and JBC-2 are 2-M20 rebars (reinforcement ration of 1.20%) and 2-SE SMA20 (20.6 mm diameter) rebars (reinforcement ratio of 1.33%), respectively. The plastic hinge length was calculated as 360 mm (Paulay and Priestley 1992) from the face of the column. Mechanical couplers

were used in JBC-2 to connect SMA rebars and regular steel rebars (Fig. 3). The total length of SMA rebars was 450 mm (centre to centre of the couplers), as shown in Fig. 3a.The ties of the beams were spaced at 80 mm for 800 mm length adjacent to the column and then spaced at 120 mm. The size of the longitudinal rebar and the size and spacing of the transverse reinforcement for the joint conform to current code requirements (CSA A23.3-04).

Regular single barrel type screw lock couplers have been used for connecting steel rebars and SMA rebars. Mechanical couplers were chosen because of the difficulty in machining and welding of SMAs. The couplers used are compatible with reinforcing bars that comply with ASTM A 615, ASTM A 706, ASTM A 996 (Barsplice Products Inc. 2006). They consist of smooth, shaped, steel sleeves with converging sides. Each end of the reinforcing bars is inserted into one of the coupler ends until it reaches the middle pin, both rebars meet head to head separated by a pin at the middle. Screws are used to hold the rebars, which are tightened until their heads are sheared off indicating that the required torque is reached. Figure 4 illustrates the couplers used in the reinforcement caging of JBC-2. The coupler was tested in the universal testing machine with SMA rebar at one end and steel rebar on the other end, Fig. 4b. To minimize the relative slippage between the rebars and the coupler and allow the SMA rebar to reach its full superelastic stress range, it was found that nine-5 mm diameter flat end screws and five-5 mm diameter sharp end screws should be used for the SMA and steel rebars, respectively.

3.2 Materials

Both specimens were cast with highly flowable ready-mix concrete with a slump of 720 mm (inverted cone method). The air content of fresh concrete was 5.5%. The concrete compressive strength at the time of testing was 53.5 MPa and 53.7 MPa for specimens JBC-1 and JBC-2, respectively. The split cylinder tensile strength for JBC-1 and JBC-2 was 3.5 and 2.8 MPa, respectively. Tensile strength tests of steel rebars were also performed in the laboratory. The yield strength, ultimate strength, and Young's modulus were 520 MPa, 630 MPa, and 198 GPa for JBC1-20M reinforcing bars and were 450 MPa, 650 MPa, and 193 GPa for JBC2-20M bars. For both specimens, the steel rebars used for ties were 10M with a yield strength and ultimate strength of 422 MPa and 682 MPa, respectively.

An extensive research of the open literature indicates that this study involves the first attempt to use SMAs as reinforcement in RC BCJs. SMAs are unique alloys with the ability to undergo large deformations and return to its original shape through stress removal (superelasticity) or heating (shape memory effect). Among a number of SMAs, Ni-Ti alloys, in particular, have distinct thermo-mechanical properties including superelasticity, shape memory effect, and hysteretic damping.

Hot-rolled Ni-Ti alloy rebar has been used as reinforcement in JBC-2 specimen. The composition of all of the samples was nearly identical, with an average of 55.0% nickel and 45.0% titanium by weight. Its austenite finish temperature, A_f, defining the complete transformation from martensite to austenite, ranges from -15ºC to -10 ºC. Above this

temperature, the alloy is within the superelastic range. Each Ni-Ti bar used in this study was 450 mm long and 20.6 mm in diameter. Each end of the rebar was inserted into the coupler over a length of 45 mm. Figure 5a shows the typical stress-strain behaviour of SMA along with steel. This figure also shows the cyclic tensile behaviour of SMA up to its superelastic strain range, where the characteristic tress-strain curve shows a flag-shaped response. Some distinctive features can be recognized in the SMA stress-strain curve of Fig. 5a: (a) elastic response of austenite material at low strains ($\varepsilon \approx 1\%$) as denoted by OP; (b) stress-induced transformation from austenite to martensite with a long and constant stress plateau at intermediate strains ($\varepsilon = 2\text{-}6\%$), indicated by PQ; (c) elastic recovery of strain upon stress removal as shown by QR; (d) instinctive recovery of strain at an almost constant stress path because of the reverse transformation to austenite due to instability of martensite as depicted by RS; and finally (e) elastic recovery in the austenite phase as indicated by SO. This exceptional property of SMA in recovering substantial inelastic deformation upon unloading yields a characteristic hysteresis loop known as superelasticity. Figure 5b shows the experimental cyclic tensile behaviour of a Ni-Ti bar within couplers at room temperature. The yield point (P in Fig. 5a) is identified as 401 MPa (f_{y_SMA}) at 0.75% strain (ε_y). Although SMA does not have a yielding process, yield is being used to refer to the initiation of phase transformation of SMA. Its low yield strength, which is 10.9% less than that of steel, is compensated by a larger SMA bar diameter of 20.6 mm compared to the 19.5 mm diameter of steel rebar. The size of SMA rebar was also chosen such that the SMA section had lower moment carrying capacity compared to that of steel section and yielding does not initiate in the steel rebar. Its Young's modulus (E) is calculated as 62.5 GPa. The rebar was tested up to a maximum

of 6% strain and a residual strain of 0.73% was observed. Since SMA modulus of elasticity is one-third that of steel, SMA is expected to experience higher strains than steel at a similar load levels.

3.3 Test setup and instrumentation

Both BCJs were tested under constant axial load applied at the top of the column and reversed quasi-static cyclic load applied at the beam tip. Figure 6 shows the typical deflected shape of the specimen under reversed cyclic loading. The load history applied at the beam tip was divided into two phases. It started with a load-controlled phase followed by a displacement-controlled loading phase. During the load-controlled phase, two load cycles were applied at 10% of the theoretical yield load of the beam to ensure that the data acquisition system is functioning properly. The following load control cycles (4 cycles) were applied to define the loads causing flexural cracking in the beam (2 cycles) and yielding of its longitudinal rebars (2 cycles). The yield load, P_y, and the yield displacement, Δ_y, were recorded. After yielding, displacement-controlled loading was applied in the form of incremental multiplies of the yield displacement, Δ_y. For each load cycle, the test specimen was subjected to two complete cycles to verify its stability. Tests were conducted up to a storey drift of 7.9%, which is more than double the collapse limit (Elnashai and Broderick 1994).

The specimen, the test rig, and the reaction frame are shown in a schematic diagram in Fig. 7. The bottom of the column was hinged with pins penetrating through a sleeve with narrow holes, whereas a roller support was created at the top of the column with pins

penetrating through a sleeve with 20 mm vertical slots. These slots permitted vertical deformation of the column and transmission of its axial load from the hydraulic jack to the lower hinge support. The load cycles were applied at the beam tip using an actuator, which was pin connected at the beam-tip. The arm length was measured as 1870 mm from the pin connection to the mid column line.

Figure 7 also illustrates the instrumentation of test specimens. Two load cells were used to measure the column axial load and beam tip load. During testing, displacements were measured at various locations using four linear variable displacement transducers (LVDTs). One pair of LVDT was attached to the joint area to measure the joint distortion. The other two LVDTs were placed in parallel on top and bottom of the beam at 180 mm away from the column face to measure beam rotation. A string potentiometer was used to measure the displacement at the free end of the beam. For both BCJ specimens, electrical resistance strain gauges were installed on the main reinforcing bars and transverse reinforcement of the beam and column as shown for JBC-2 in Fig. 3a. Data generated from different monitoring devices were segregated into analogue (load cells, LVDTs) and digital (strain gauges) feeds, which were connected to the data acquisition system. A portable computer attached to the data acquisition system was used to record readings at a constant time interval with one reading per second.

4. Experimental Results

4.1 Specimen JBC-1

Figure 8a shows the beam tip load versus storey drift relationship of specimen JBC-1. The first flexural crack was observed at the top of the beam near the column face at a beam tip-load of 11.7 kN corresponding to a drift of 0.22%. The first diagonal crack in the joint appeared close to the first flexural crack at a beam tip load of 30.0 kN corresponding to a drift of 0.66 %. Additional cracks occurred at the joint with the progress of loading. However, all the cracks in the joint region were of very fine width streaming from the first two cracks that emerged along the diagonals. The top longitudinal rebar of the beam first yielded at a beam tip-load of 51.3 kN with a corresponding yield displacement, Δ_y of 12 mm (drift of 1.3%). At a displacement of $2\Delta_y$ (2.6% drift), the beam suffered a relatively wide flexural crack at the column face that extended its full depth along with some minor cracks that formed parallel to the column face. At a displacement ductility of $4\Delta_y$ (5.2% drift), the crack at the column face widened and two relatively large cracks almost parallel to the column face became more evident at distances of approximately 180 mm and 300 mm from the column face. At this stage, some concrete cover at the bottom of the beam close to the column face started to spall off. At a deformation level of $6\Delta_y$, the beam became extensively cracked at the plastic hinge region over a length of 300 mm with several large cracks reaching a width of 1.7 to 2.6 mm. Some concrete cover from the bottom part of the beam also spalled off as shown in Fig. 9a. Throughout the test, the axial load of the column was maintained and the joint area remained fully undamaged apart from few hairline cracks (Fig. 9a and 9b).

4.2 Specimen JBC-2

Figure 8b shows the load-storey drift relationship of the SMA-RC beam-column joint specimen JBC-2. The First Flexural Crack (FFC) was detected at the bottom of the beam at 160 mm away from the column face at a drift of 0.22%. In the subsequent cycle that was having the same drift, another crack developed at the top of the beam at a distance of 197 mm away from the column face and extended meeting the first crack. Thus, a single fine crack is formed that extended over full beam-depth. With the progress of loading several flexural cracks occurred at the top and bottom of the beam along a length of 1300 mm measured from the column face. At a beam tip-load of 18 kN and a drift of 0.66%, a small crack appeared at the bottom edge of the joint region near the column face. A fine crack took place along the diagonal of the joint at a beam tip-load of 22 kN corresponding to a drift of 1.12%. It was observed that the bottom SMA rebar reached its yield strain at a beam tip-load of 32.7 kN and a drift of 1.97%. In this case, the corresponding yield displacement, Δ_y was found as 18 mm. At a deformation level of $2\Delta_y$, the existing flexural cracks started to propagate further deeper into the beam. Some minor cracks streamed out of the FFC toward the column face. The FFC also started to grow wider and reached a width of 5.3 mm at the outer face. When the displacement cycle reached to zero, the crack width at the plastic hinge region became smaller and it was even less than 0.5 mm. At a deformation level of $3\Delta_y$, the FFC opened up to 7.4 mm and later closed to a width of less than 1 mm. Several existing flexural cracks in the beam extended to its full depth parallel to the column face. At a deformation level of $4\Delta_y$, the cracks became wider in the plastic hinge area of the beam. The FFC opened up to 10.7 mm during the loading cycle, and part of the bottom concrete cover spalled off. At the

end of this cycle, the residual FFC crack width was 2.2 mm, whereas all other cracks in the beam had very small width. The joint region was having few diagonal cracks of very fine width and small length and remained almost fully intact. Figures 9c and 9d show the crack pattern of JBC-2.

4.3 Load-storey drift envelope

Figure 10 shows the beam-tip load versus storey drift envelope of two tested specimens JBC-1 and JBC-2. Both envelopes exhibited typical elasto-plastic behaviour. They started with comparable initial stiffness. The curve for JBC-2 shows a drop in its stiffness after the first flexural crack because of the SMA's lower Young's modulus compared to that of steel. However, both specimens maintained stable post-yield load carrying capacity, and beyond 4% drift both specimens exhibited similar load carrying capacities. Thus, at the final test stage of 7.9% drift, the beam tip-load of JBC-1 was only 2.5% lower compared to that of JBC-2.

4.4 Cumulative energy dissipation

The cumulative energy dissipated by the specimens during reversed cyclic loading was calculated by summing up the dissipated energy in successive load-displacement loops throughout the test. The cumulative energy dissipation with respect to storey drift for specimens JBC-1 and JBC-2 is presented in Fig. 11. JBC-1 dissipated 3.4 kN.m of energy at a storey drift of 3% (collapse limit as defined by Elnashai and Broderick 1994), whereas JBC-2 dissipated 2.4 kN.m of energy. At a storey drift of 3.7 %, JBC-2 dissipates equivalent amount of energy to that dissipated by JBC-1 at a storey drift of

3.0%. The amount of energy dissipated at 4% storey drift for JBC-1 is equivalent to the amount of dissipated energy by JBC-2 at a storey drift of 5.4%. At a storey-drift of 7.9%, JBC-1 was found to absorb 26.5 kN.m of energy, whereas JBC-2 dissipated 16.7 kN.m of energy at the same storey-drift, which is similar to the energy dissipated by JBC-1 at 6% storey drift. The results show that JBC-2 dissipated 37% less energy compared to that of JBC-1 at 7.9% storey drift. This is because of the large hysteretic loop of steel compared to that of the SE SMA material. This is also evident by the different shapes of the individual hysteretic loops of the load-displacement curves of the tested specimens (Fig. 8). The level of damage in JBC-1 indicates that the steel RC joint suffered extensive cracking in the beam hinge region (Fig. 9a and 9b), which helped to dissipate a higher amount of energy, whereas the SMA-RC joint suffered moderate and localized damage (Fig. 9c and 9d).

4.5 Beam rotations

Beam rotations were measured at the plastic hinge region using two LVDTs mounted on top and bottom of the beam at a distance of 180 mm from the column face (Fig. 7). The beam rotations with respect to the applied moment for JBC-1 and JBC-2 are presented in Figs. 12a and 12b, respectively. Figure 13 shows the positive moment and beam rotation envelopes of both specimens. The results depict that specimen JBC-2 had a significant amount of rotation before yielding of SMA compared to that of JBC-1. This increase in rotation is mainly due to the lower stiffness of SMA rebar compared to that of steel. Although both specimens were subjected to an equal amount of storey-drift (7.9%), JBC-2 experienced larger beam rotations of 0.0183 rad compared to 0.0101 rad for JBC-1.

However, JBC-1 suffered higher residual beam-rotation (0.00093 rad) compared to that of JBC-2 (0.00052 rad).

4.6 Measured strains in rebars

Strains were measured in longitudinal and transverse reinforcing bars. Figures 14a and 14b show the measured strains in the main top reinforcing steel and SMA rebar at the plastic hinge region, close to the column face of specimens JBC-1 and JBC-2, respectively. Figures 14c and 14d show the measured strains in the main bottom reinforcing steel and SMA bar of specimens JBC-1 and JBC-2, respectively. Figures 14a and 14c show that specimen JBC-1 suffered high residual strain both in the bottom and top bars beyond its yield load, whereas Figs. 14b and 14d illustrate that JBC-2 experienced negligible residual strain even when it was subjected to larger strain. However, strains in the steel and SMA rebar could not be recorded till the end of the test since strain gauges were damaged at approximately 5.1% and 4% storey-drift of JBC-1 and JBC-2, respectively. For specimen JBC-2, SMA rebars were placed close to the face of the column and its low modulus of elasticity compared to that of steel resulted in higher strain in the plastic hinge region, causing a major crack away from the column face. For specimen JBC-1 the maximum measured strain in the main steel reinforcing rebar inside the joint was 2066 micro-strain with larger loops of strain, whereas the steel reinforcing rebar inside the joint of specimen JBC-2 experienced only 1156 micro-strain with smaller loops. This might be due to transferring a portion of the force in the SMA rebar to the concrete through bearing of the coupler.

The maximum measured strain in the transverse reinforcement inside the joint of JBC-1 was 1291 micro-strain, while the corresponding maximum value for specimen JBC-2 was about 990 micro-strain. This difference in the strain distributions is likely due to the use of smooth SMA rebars in JBC-2 that experienced slippage at the face of the joint and changed the distribution of shear strains within the joint. This might have also helped in developing a plastic hinge region away from the column face. Figures 15a and 15b show the strains in the transverse reinforcement closest to the major crack of specimens JBC-1 and JBC-2, respectively. It is quite evident that JBC-2 suffered much lower strains compared to that of JBC-1. Strains were also measured on main reinforcing bars and stirrups of columns for both specimens at a distance of 615 mm and 560 mm away from the beam bottom face, respectively. For both specimens, the maximum strain in the column longitudinal bar was less than 200 micro-strain, whereas in the stirrup it was less than 50 micro-strain.

5. Discussion

The use of SMA as reinforcement in concrete is yet to be introduced in real structural applications. Before establishing SMA as reinforcement, various design guidelines and provisions need to be developed for its safe implementation in large-scale field applications.

Although there is a substantial potential for utilizing SMA as concrete reinforcement, the cost of this material is a primary restraining factor to its implementation. However, there has been a significant reduction in the prices of Ni-Ti over the last ten years, from more

than 1000 USD to below 150 USD per kg at present. The price is still considerably higher than that of other construction materials. However, SMA can be used along with steel in a hybrid system, thus achieving a cost competitive design with several performance gains. Screw lock coupler that costs about 60 USD after machining was used for connecting SMA with steel. It has several advantages over a threaded coupler since it does not require threading or special treatment to the ends of the rebars. No special installation equipment is required; quick and easy installation save time and money, which is ideal for new construction.

SMA rebars available in the market have smooth surfaces, providing lower bond strength to concrete compared to that of steel. If SMA alone is used as reinforcement, this may impose difficulties in design, for instance, in satisfying the rebar development length. Fe-based SMAs are cheap (Janke et al. 2005) and may have better bond strength compared to that of Ni-Ti when used as reinforcing bars in RC structures. The problems related to these alloys include poor shape recovery and low shape recovery stress. Sand coating on the rebar surface can also improve the bond strength (Chang et al. 2002) between SMA and concrete. Use of couplers may also help in improving the bond capacity as they position themselves permanently in the joint region with no displacement.

Another disadvantage of SE SMA-RC structures is its lower energy dissipation capacity compared to that of steel-RC structures under earthquake loading, as demonstrated by the performance of JBC-2 and JBC-1. Past studies have shown that the large diameter SMA bars tend to have much lower equivalent viscous damping compared to wires (DesRoches et al. 2004). Although SE SMA rods dissipate a lower amount of energy, the advantage is

that they can dissipate a considerable amount of energy under repeated load cycles with negligible residual strains. Generally, the loading plateau and the hysteretic loop gradually decrease and the residual strain increases for successive loading cycles of SE SMA due to localized slip. However, this behaviour has been proven to decrease and stabilize at a large number of cycles (Miyazaki et al. 1986).

The present study focused on studying the performance under reversed cyclic loading of concrete BCJs reinforced with SE SMA at their plastic hinge region. Besides code specified regular reinforcement detailing of BCJs, there are different approaches in the literature for improved ductility and damage tolerance of the joints. For instance, use of headed bars at the joint region can relocate the plastic hinge away from the column face (Chutarat and Aboutaha 2003), use of additional diagonal bars at the joint can result in enhanced strength and improved bond condition in the joint (Au et al. 2005), use of high performance fibre-reinforced cement composites at the joint area can improve the damage tolerance (Parra-Montesinos et al. 2005). All of these methods experience large residual-drift at the end of seismic loading. Conversely, the main advantage of using SE SMA in specimen JBC-2 is its low residual storey-drift at the end of cyclic loading and formation of plastic hinge away from the column face. The maximum residual storey drift for JBC-2 was 1.98% whereas for JBC-1, the value was 4.94%. Similar behaviour was observed while using superelastic SMA as reinforcement in the plastic hinge region of concrete column under dynamic loading (Saiidi and Wang 2006). Thus, SE SMA-RC structures are expected to dissipate a significant amount of energy under earthquake loading, but potentially regain its original shape upon stress removal, thus requiring

minimum repair. Full-scale dynamic tests on hybrid concrete frames reinforced with SE SMA at its plastic hinge regions and steel in other regions need to be conducted to assess its performance and the associated progress of global failure. The results can be used to calibrate numerical models that can be used to simulate the behaviour of such SE SMA-RC multi-storey concrete frames with high degrees of redundancy, and accordingly predict the progress of failure and its performance under earthquake loading. The numerical results can also be used for performance-based design guidelines. Devoted research efforts are still required to address many issues and uncertainties before the widespread use of SMA as concrete reinforcement to make it safe and competitive in seismic areas for large-scale structural applications.

6. Conclusions

The use of SE SMA rebars in the plastic hinge region of a BCJ has been examined under reversed cyclic loading. The experimental investigation described in the present paper provides an insight into the potential for developing a new type of RC structures with hybrid steel-SMA reinforcement. Based on the experimental observations and analysis of test results, the following conclusions can be drawn.

1. The flag-shaped hysteretic stress-strain curve of SE SMA rebar produced a flag-shaped force-displacement hysteretic shape for JBC-2. This resulted in very small residual displacements in the SE SMA-RC beam-column joint JBC-2 compared to that of the conventional steel-RC beam-column joint JBC-1. This extraordinary characteristic of SE

SMA-RC beam-column joints could have a great benefit in highly seismic areas, where such RC joints would remain functional even after a strong earthquake.

2. In the case of steel-RC beam-column joint specimen JBC-1, the plastic hinge developed at the face of the column. On the other hand, the use of SE SMA in the joint region of JBC-2 successfully relocated the plastic hinge region away from the column face to a distance of approximately half of the beam-depth.

3. Specimen JBC-2 dissipated lesser amount of energy compared to that of JBC-1. However, it could dissipate equivalent amount of energy of JBC-1 at an expense of relatively larger storey drift . Larger hysteretic loop of steel and extensive cracking in concrete in the beam hinge region of JBC-1 resulted in higher amount of energy dissipation compared to that of SE SMA-RC BCJ specimen JBC-2.

4. The beam moment rotation relationship of JBC-2 was found different than that of JBC-1 because of the low modulus of elasticity of SMA, which led to delayed yielding of the Ni-Ti rebar compared to that of steel. This also caused higher beam rotation in JBC-2 than that of JBC-1 at equivalent beam-tip displacements.

5. The strains in the longitudinal SMA rebar of specimen JBC-2 experienced negligible residual strain, while longitudinal steel rebar of specimen JBC-1 suffered much larger residual strain. The transverse reinforcements inside the joint of specimen JBC-1 also experienced larger strains compared to that of JBC-2.

The study mainly focused on observing the performance of subassemblies and their level of damage during reversed cyclic loading. It should assist in developing a numerical model, which will be able to simulate the performance of SE SMA-RC beam column joints. Such a model can be used to assess the performance of SE SMA-RC multi-storey frames under dynamic loading, allowing predicting their capacities and meeting seismic resistance requirements. It is also important that the design code provisions for seismic design of steel-RC structures are re-examined for SMA-RC structures considering its low modulus of elasticity, low energy dissipation capacity, large deformation capability, negligible residual strain, and recentering capability.

Acknowledgement

References

Alam, M.S., Youssef, M.A. and Nehdi, M. (2007a) "Utilizing shape memory alloys to enhance the performance and safety of civil infrastructure: a review," *Canadian Journal of Civil Engineering*, 34(9), 1075-1086.

Alam, M.S., Nehdi, M. and Youssef, M.A. (2007b) "Shape memory alloy based smart RC bridge: overview of state of the art," *Smart Structures and Systems, An International Journal*, in press.

A615/A615M-06a. Standard specification for deformed and plain carbon-steel bars for concrete reinforcement. West Conshohocken (PA), ASTM Intl 2007.

A706/A706M-06a. Standard specification for low-alloy steel deformed and plain bars for concrete reinforcement. West Conshohocken (PA), ASTM Intl 2007.

A996/A996M-06a. Standard specification for rail-steel and axle-steel deformed bars for concrete reinforcement. West Conshohocken (PA), ASTM Intl 2007.

Au, F.T.K., Huang, K., and Pam, H.J. (2005) "Diagonally-reinforced beam-column joints reinforced under cyclic loading," Proceedings of the Institution of Civil Engineers: Structures and Buildings, 158(1), 21-40.

Barsplice Products Inc. (2006) "Zap Screwlok ® Mechanical splices and connectors for reinforcing bars – review," visited on April 08, 2006, available at: http://www.barsplice.com/BPI_Scans/Zap_Data-Sheet_RevA.pdf.

Chang, J.J., Yeih, W. and Tsai, C. L. (2002) "Enhancement of bond strength for epoxy-coated rebar using river sand," *Construction and Building Materials*, 16(8), 495-472.

Chutarat, N., and Aboutaha, R.S. (2003) "Cyclic response of exterior reinforced concrete beam-column joints reinforced with headed bars - Experimental investigation," *ACI Structural Journal*, 100(2), 259-264.

Clark, P.W., Aiken, I. D., Kelly, J. M. Higashino, M. and Krumme, R. (1995) "Experimental and analytical studies of shape-memory alloy dampers for structural control," *Proc. of SPIE*, Vol. 5, pp. 241-251.

CSA A23.3-04 (2004) *Design of Concrete Structures* (Canadian Standards Association, Rexdale, Ontario, Canada).

DesRoches, R. and Delemont, M. (2002) "Seismic retrofit of simply supported bridges using shape memory alloys," *Engineering Structures*, 24(3), 325-332.

DesRoches, R., McCormick, J., and Delemont, M. (2004) "Cyclic properties of superelastic shape memory alloy wires and bars," *Journal of Structural Engineering,* 130(1), 38–46.

Dolce, M., Cardone, D., Marnetto, R., Mucciarelli, M., Nigro, D., Ponzo, F.C. and Santarsiero, G. (2004) "Experimental static and dynamic response of a real RC frame upgraded with SMA re-centering and dissipating braces," *Proc. of the 13th World Conf. on Earthquake Engg.*, Canada, paper no. 2878.

Elnashai, A.S. and Broderick, B.M. (1994) "Seismic resistance of composite beam-columns in multi-storey structures. Part 1: Experimental studies," *Journal of Constructional Steel Research*, 30(3), 201-229.

Inaudi, J. A. and Kelly, J. M. (1994) Experiments on tuned mass dampers using viscoelastic, frictional and shape memory alloy materials," *Proc. First World Conf. on Structural Control*, Vol. 2(TP3), pp. 127-136.

Indirli, M., Castellano, M.G., Clemente, P., and Martelli, A., 2001. Demo-application of shape memory alloy devices: The rehabilitation of the S. Giorgio Church Bell-Tower," *Proc. of SPIE*, Vol. 4330, pp. 262-272.

Janke, L., Czaderski, C., Motavalli, M., and Ruth, J., (2005) "Applications of shape memory alloys in civil engineering structures – overview, limits and new ideas," Materials and Structures, 38(6), 578-592.

Maji, A.K. and Negret, I (1998) "Smart prestressing with shape memory alloy," *Journal of Engineering Mechanics*, 124(10), 1121-1128.

Miyazaki, S., Imai, T., Igo, Y. and Otsuka, K. (1986) "Effect of cyclic deformation on the pseudoelasticity characteristics of Ti–Ni alloys," *Metallurgical Transactions. A*, 17A, 115–120.

National Building Code of Canada, 2005, National Research Council, Canada.

Park, R. and Paulay, T. (1975) *Reinforced Concrete Structures* (John Wiley & Sons Inc, New York).

Parra-Montesinos, G.J., Peterfreund, S.W., and Chao, S.H. (2005) "Highly damage-tolerant beam-column joints through use of high-performance fiber-reinforced cement composites," *ACI Structural Journal*, 102(3), 487-495.

Paulay, T. and Priestley, M. N. J. (1992) *Seismic Design of Reinforced Concrete and Masonry Buildings* (John Wiley & Sons, Inc., New York).

Saiidi, M.S. and Wang, H. (2006) "Exploratory study of seismic response of concrete columns with shape memory alloys reinforcement," ACI Structural Journal, 103(3), 435-442.

Saatcioglu, M., Mitchell, D., Tinawi, R., Gardner, N.J., Gillies, A.G., Ghobarah A., Anderson, D.L. and Lau, D. (2001) "The August 17, 1999, Kocaeli (Turkey) earthquake - damage to structures," *Canadian Journal of Civil Engineering*, 28(4), 715-737.

Wang, H. (2004) "A study of RC columns with shape memory alloy and engineered cementitious composites," M.Sc. Thesis, Department of Civil Engineering, University of Nevada, Reno.

Wilde, K., Gardoni, P. and Fujino, Y. (2000) "Base isolation system with shape memory alloy device for elevated highway bridges," *Engineering Structures*, 22(3), 222-229.

Wilson, J.C. and Wesolowsky, M.J. (2005) "Shape memory alloys for seismic response modification: a state-of-the-art review," *Earthquake Spectra*, 21(2), 569-601.
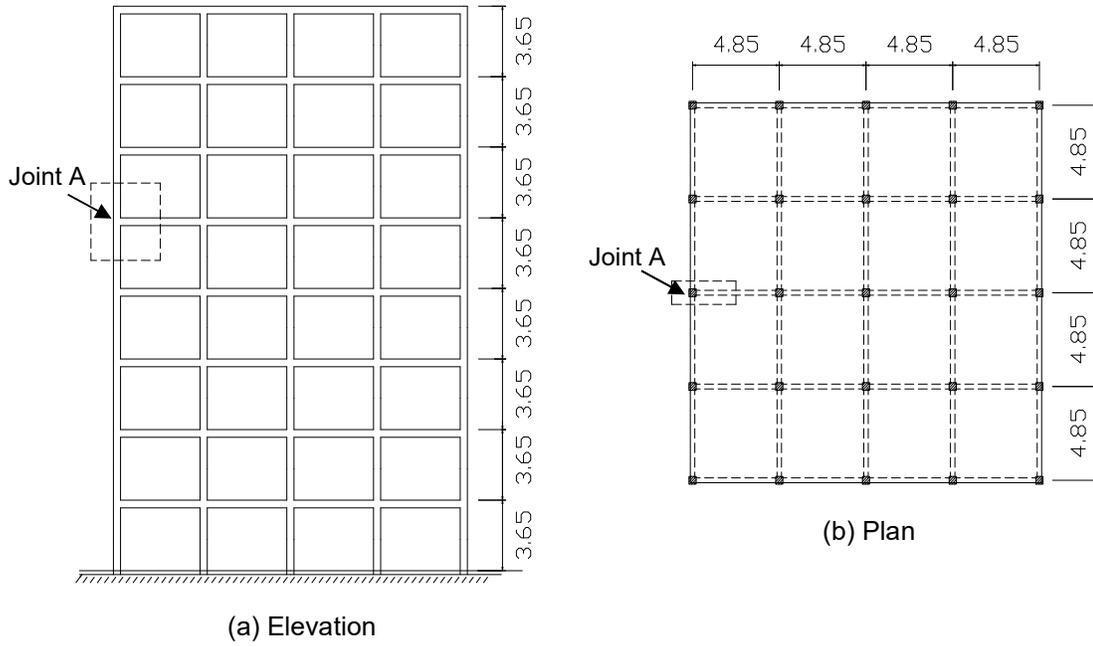
Fig. 1. Eight-storey frame building located in the western part of Canada (dimensions in meters).
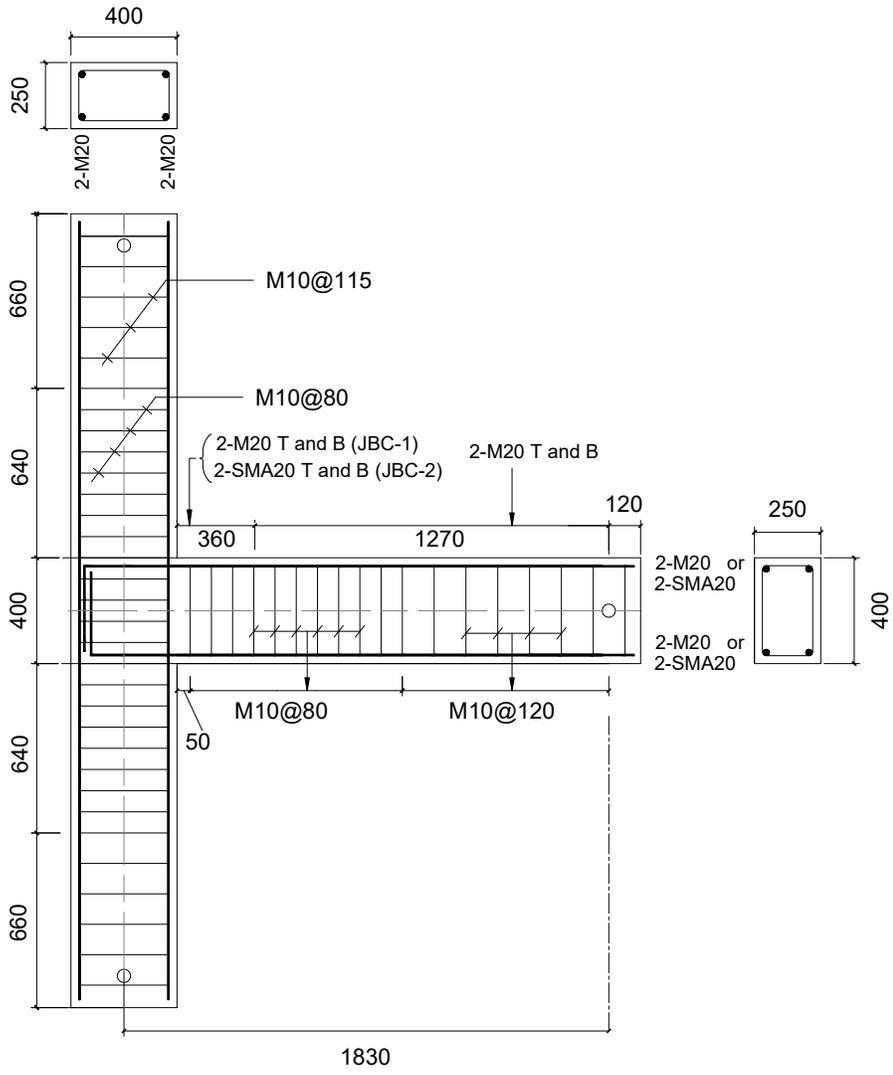
Fig. 2. Reinforcement details of specimens JBC-1 and JBC-2 (all dimensions in mm).
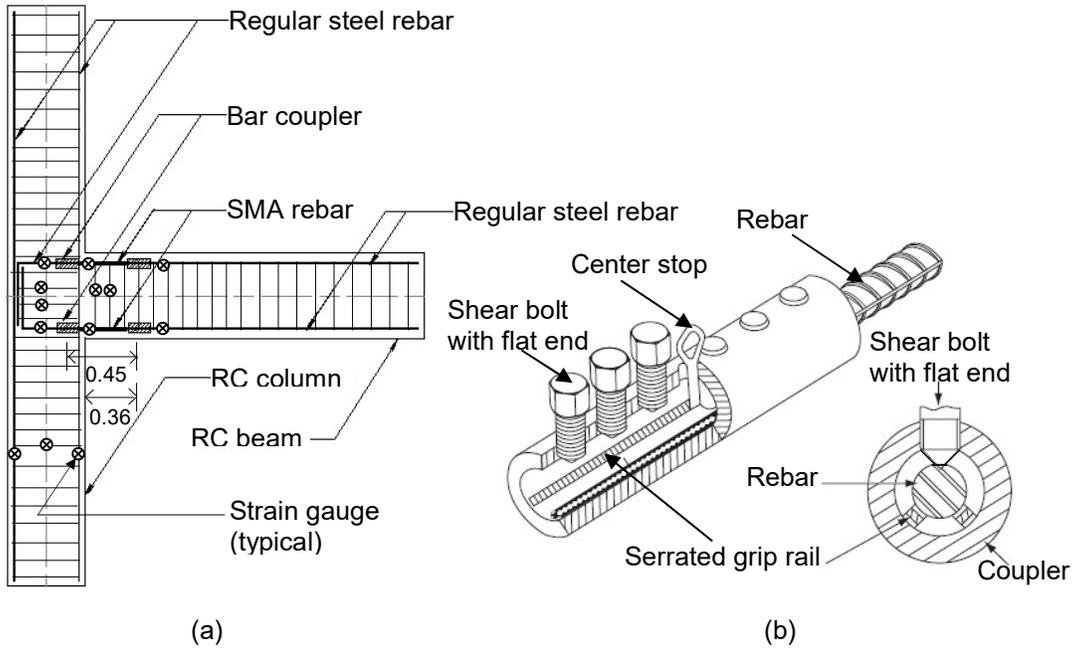
Fig. 3. (a) Splice details of specimen JBC-2 and the positions of strain gauges, (b) regular single barrel screw-lock coupler for connecting SMA rebar with regular steel rebar (all dimensions in m).
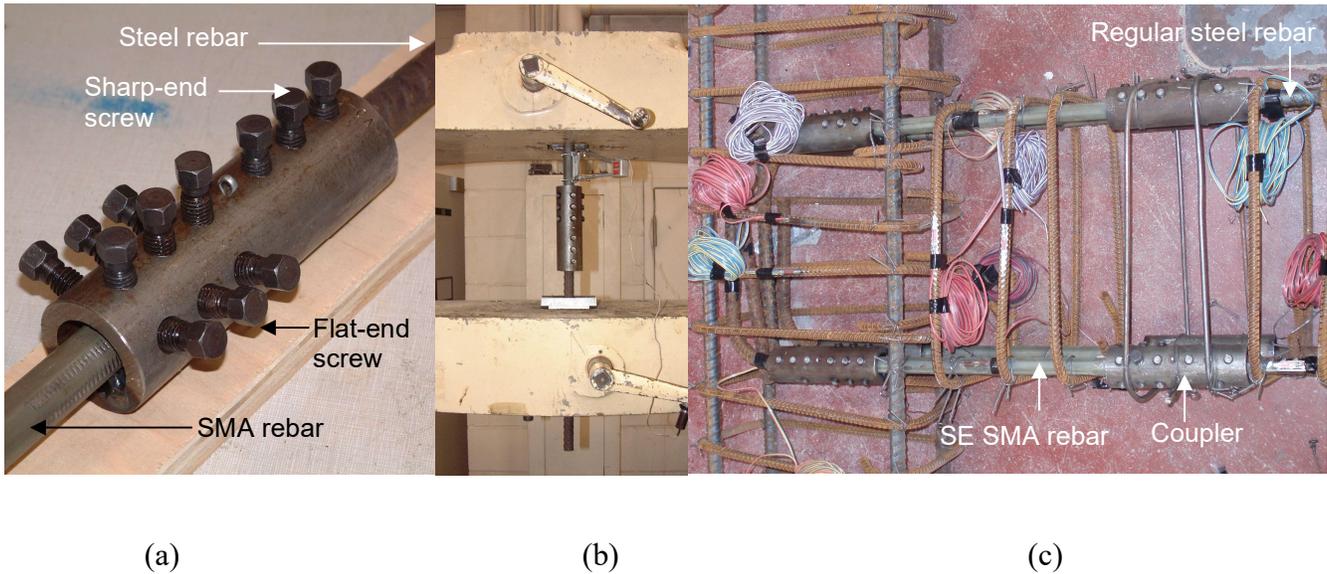
Fig. 4. (a) Coupler used in JBC-2, (b) test setup of coupler in universal testing machine, and (c) reinforcement caging of JBC-2.
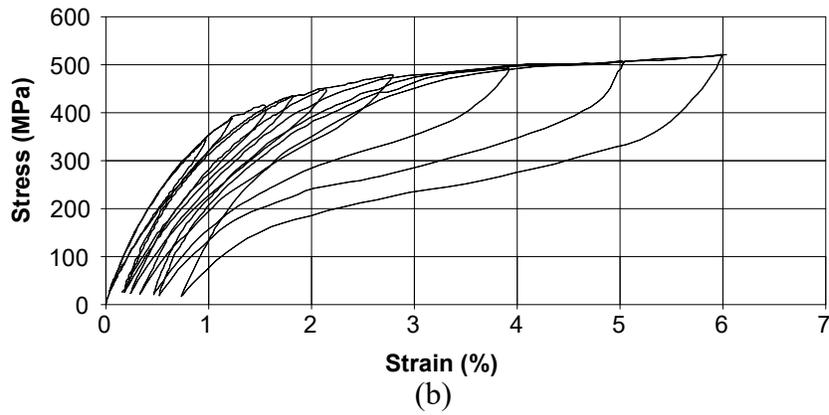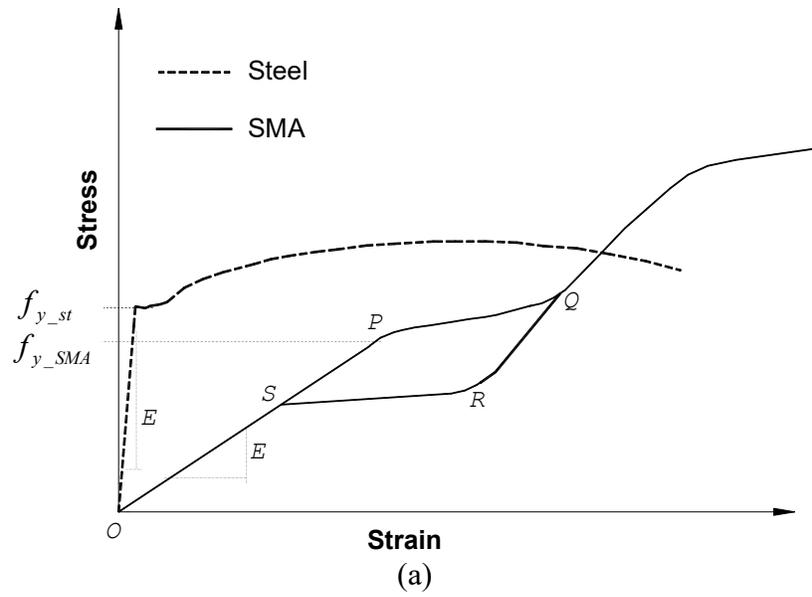
Fig. 5. (a) Typical stress-strain behaviour of SE SMA and steel; and (b) experimental cyclic tensile strength of SE SMA rebar within couplers.
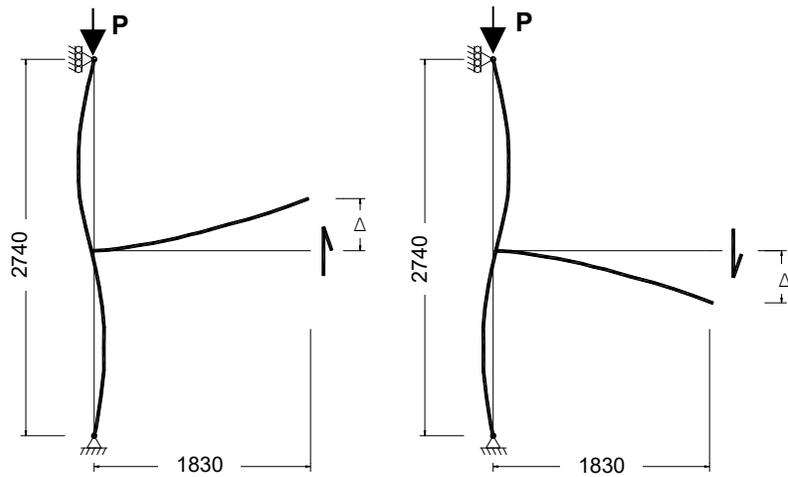
Fig. 6. Typical deflected shape of specimen under reversed cycle of beam tip displacement.
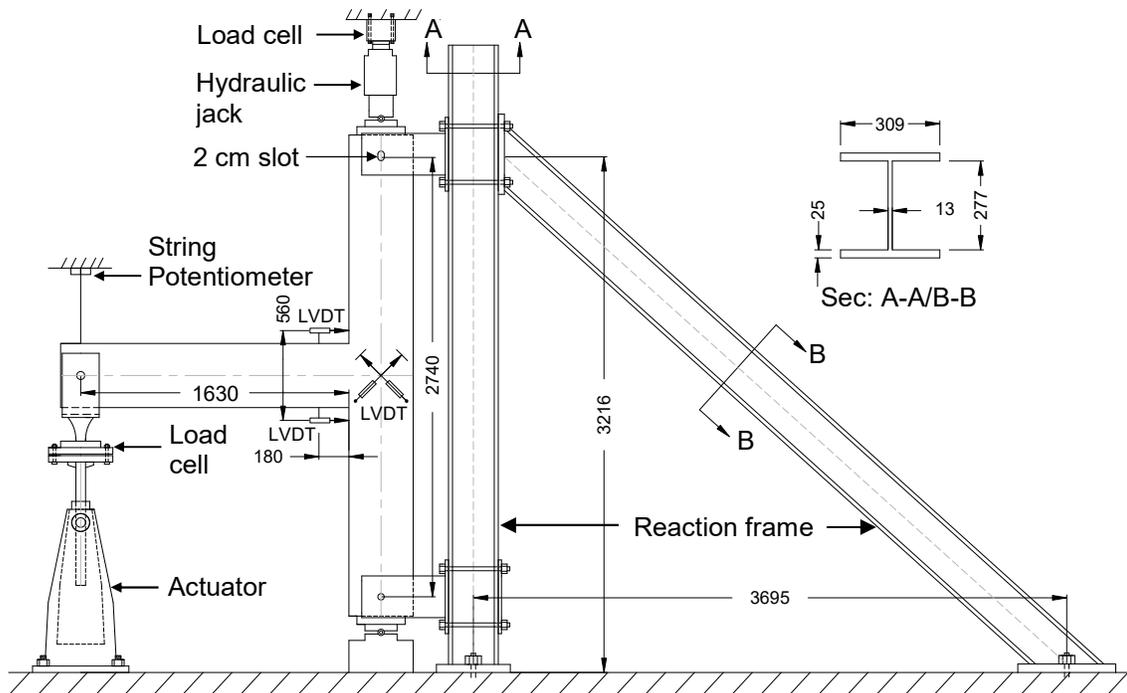
Fig. 7. Test setup (all dimensions in mm).

(a)

(b)
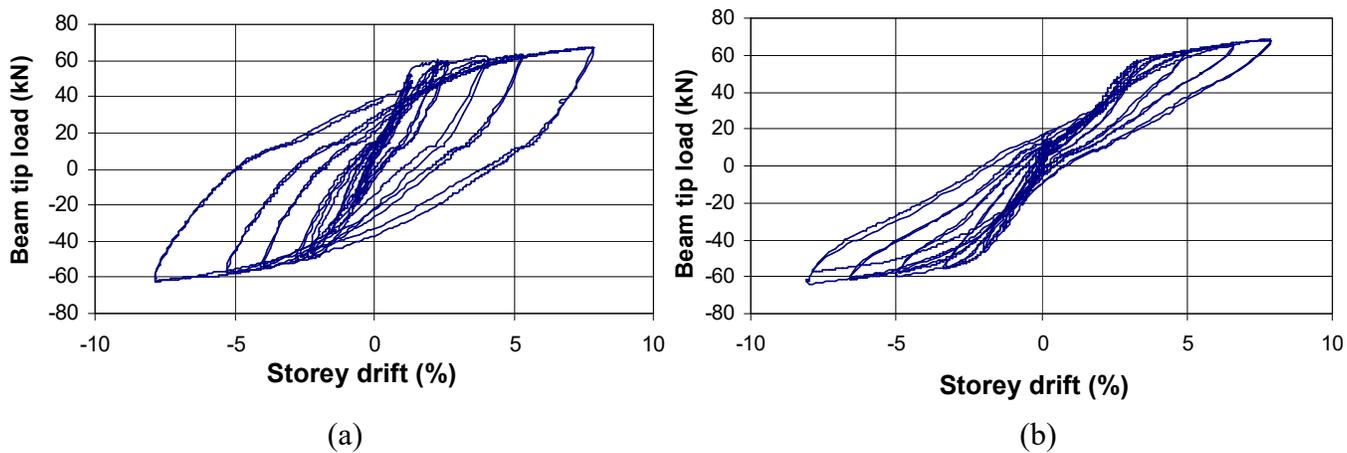
Fig. 8. Beam tip load-storey drift relationship of specimens: (a) JBC-1 and (b) JBC-2.

(a)   (b)

(c)   (d)
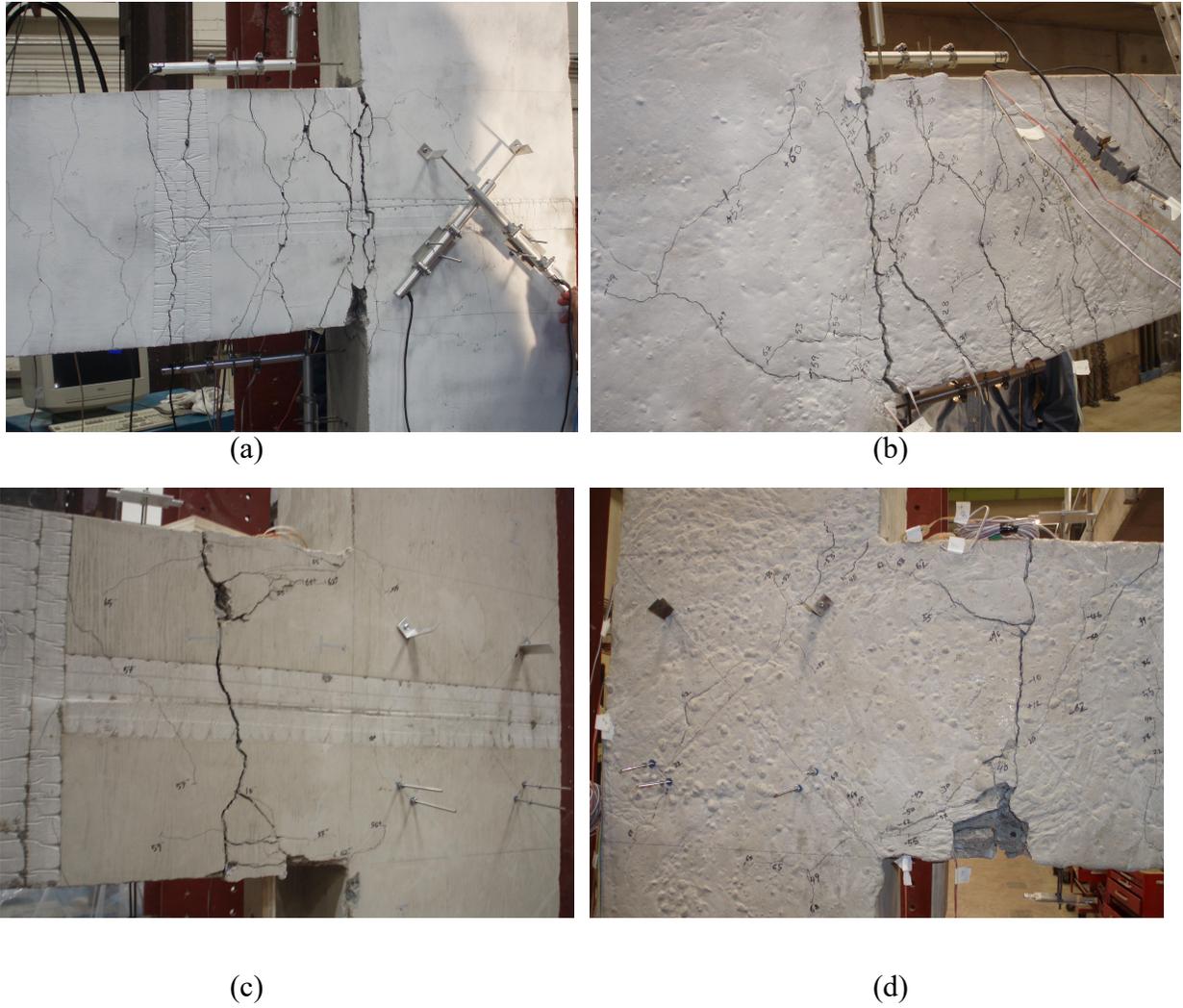
Fig. 9. Crack pattern of specimens after being subjected to cycles up to 72 mm: (a) front face of JBC-1, (b) rear face of JBC-1, (c) front face of JBC-2, and (d) rear face of JBC-2.
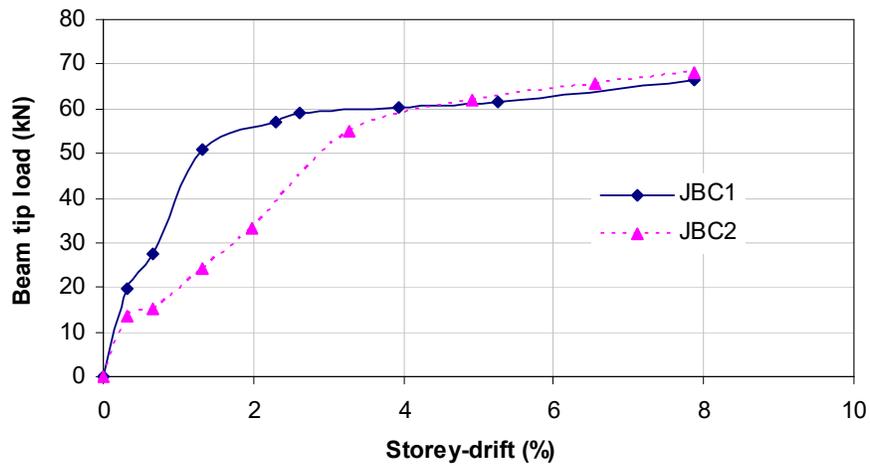
Fig. 10. Beam tip-load versus storey drift envelope of the tested specimens JBC-1 and JBC-2.
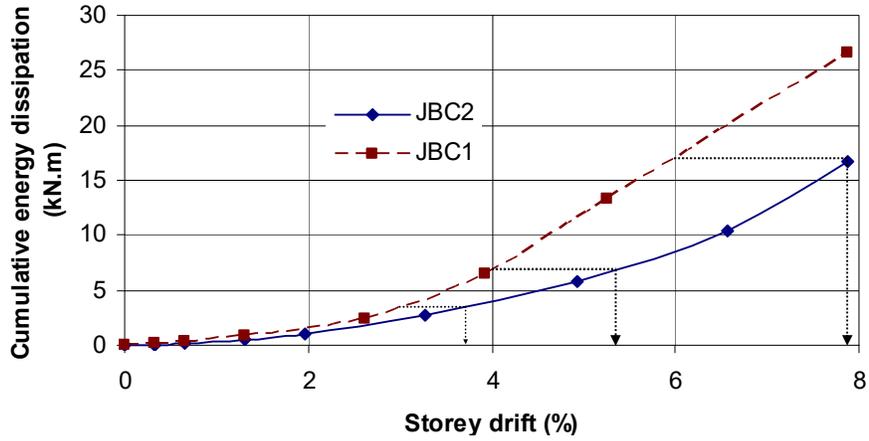
Fig. 11. Cumulative energy dissipation-storey drifts relationship of specimens JBC-1 and JBC-2.

(a)

(b)
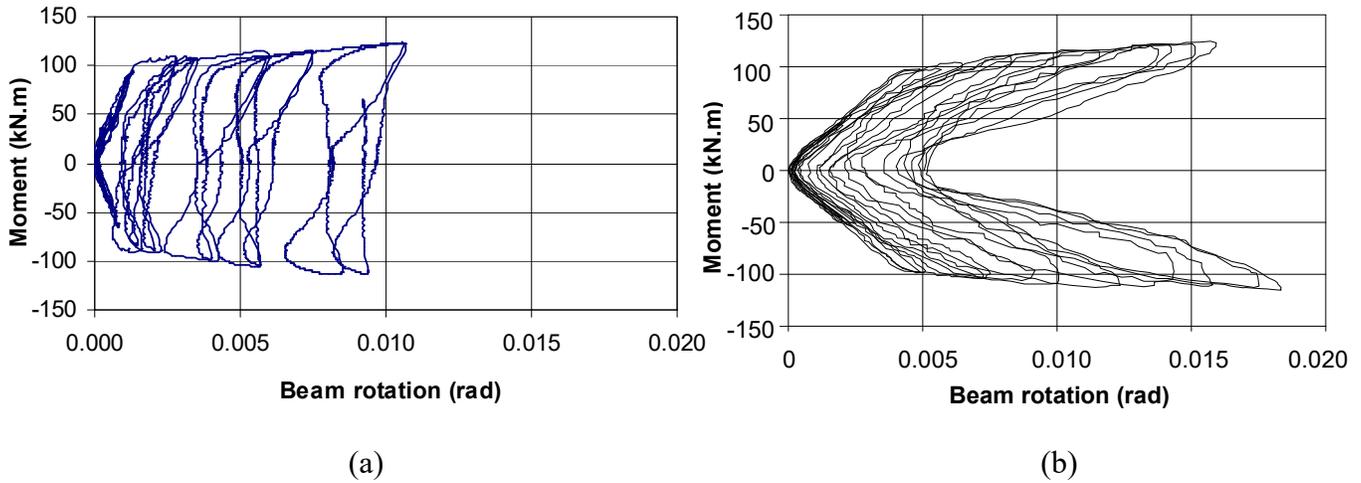
Fig. 12. Beam moment-rotation plots at 180mm away from the column face of specimens: (a) JBC-1, and (b) JBC-2.
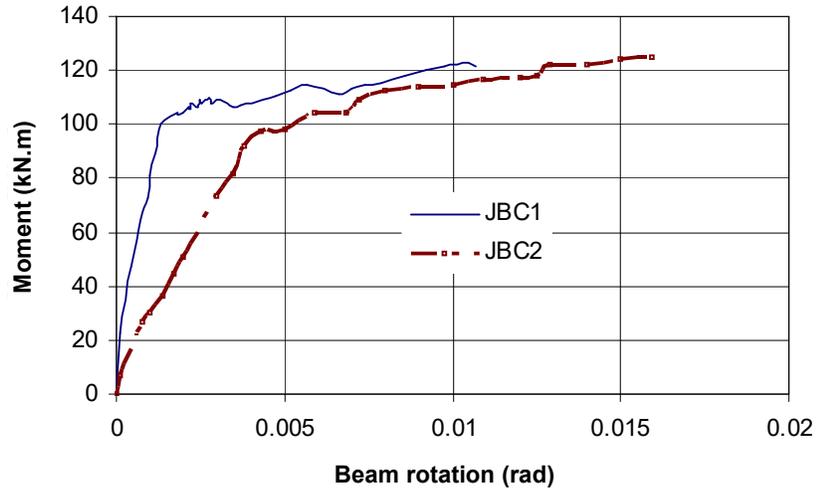

Fig. 13. Beam moment versus rotation envelope of the tested specimens.
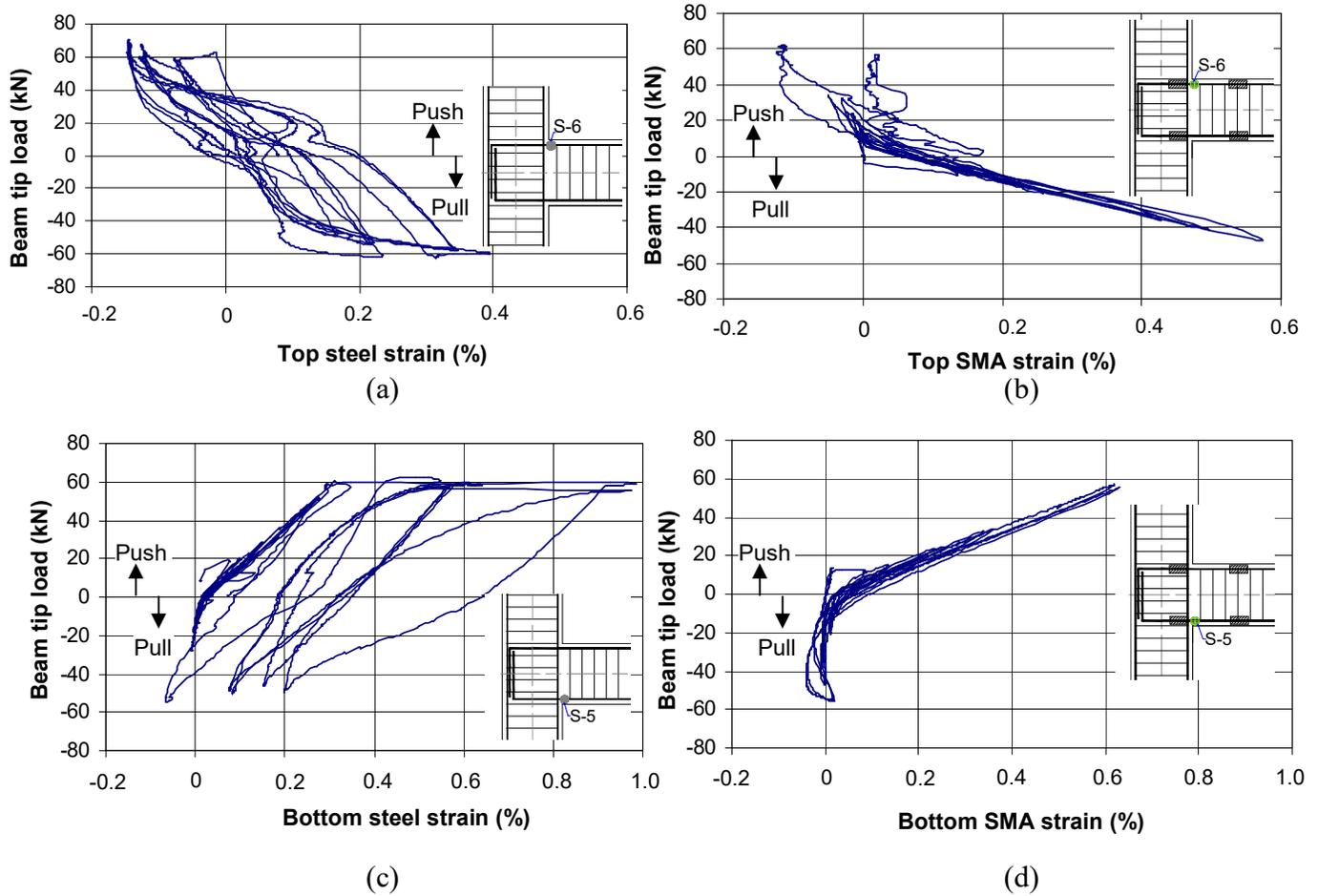
(a)

(b)

(c)

(d)

Fig. 14. Strains in main longitudinal reinforcements at the column face of joint specimens: (a) top rebar of JBC-1, (b) top rebar of JBC-2, (c) bottom rebar of JBC-1, and (d) bottom rebar of JBC-2.
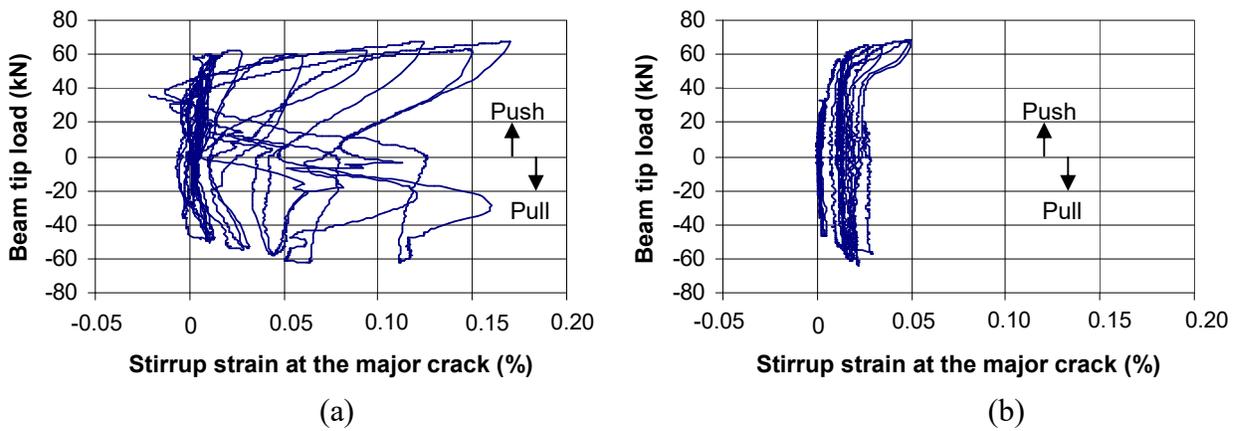

(a)

(b)

Fig. 15. Strains in transverse reinforcement at the location of major crack of specimens (a) JBC-1, and (b) JBC-2.